

pubs.acs.org/NanoLett Letter

# Resolving Electron—Electron Scattering in Plasmonic Nanorod Ensembles Using Two-Dimensional Electronic Spectroscopy

William R. Jeffries, Kyoungweon Park, Richard A. Vaia, and Kenneth L. Knappenberger, Jr.\*



Cite This: Nano Lett. 2020, 20, 7722-7727



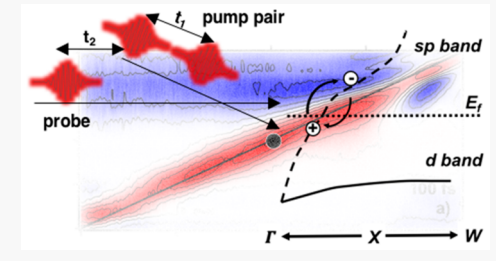
ACCESS

Metrics & More



3 Supporting Information

**ABSTRACT:** The use of two-dimensional electronic spectroscopy (2DES) to study electron–electron scattering dynamics in plasmonic gold nanorods is described. The 2DES resolved the time-dependent plasmon homogeneous line width  $\Gamma_{\rm h}(t)$ , which was sensitive to changes in Fermi-level carrier densities. This approach was effective because electronic excitation accelerated plasmon dephasing, which broadened  $\Gamma_{\rm h}$ . Analysis of  $\Gamma_{\rm h}(t)$  indicated plasmon coherence times were decreased by 20–50%, depending on excitation conditions. Electron–electron scattering rates of approximately 0.01 fs<sup>-1</sup> were obtained by fitting the time-dependent  $\Gamma_{\rm h}$  broadening; rates increased quadratically with both excitation pulse energy and frequency. This rate dependence agreed with Fermi-liquid theory-based



predictions. Hot electron thermalization through electron—phonon scattering resulted in  $\Gamma_h$  narrowing. To our knowledge, this is the first use of the plasmon  $\Gamma_h(t)$  to isolate electron—electron scattering dynamics in colloidal metal nanoparticles. These results illustrate the effectiveness of 2DES for studying hot electron dynamics of solution-phase plasmonic ensembles.

KEYWORDS: Plasmonics, hot electrons, nanoparticles, two-dimensional electronic spectroscopy, electron dynamics

wing to their large visible light extinction, plasmonic nanostructures have emerged as functional transducers for a variety of light-harvesting applications. In particular, the use of hot electrons generated by plasmon excitation to mediate chemical processes has attracted considerable interest. <sup>1–3</sup> Indeed, several examples that leverage either the electronic or thermal aspects of plasmonic excitation for photocatalysis have been reported. <sup>4–6</sup> One of the challenges of using hot electrons is the need to harvest these carriers before the excitation energy is lost to scattering channels that lead to thermalization.

In the case of gold nanoparticles, plasmon-resonant excitation leads to the phase coherent formation of a nonequilibrium Fermi gas. This electron gas equilibrates through a series of sequential steps that span the femtosecond to picosecond time scales: (i) ultrafast (~10 fs) electronic plasmon dephasing; (ii) rapid (~100 fs) electron-electron scattering; (iii) subpicosecond electron-phonon scattering; and (iv) energy dissipation to the nanoparticle surroundings over tens to hundreds of picoseconds. Because strategies for harvesting nonequilibrium electrons on ultrashort time scales (sub-100 fs) have been of heightened interest, experimental methods capable of resolving electron-electron scattering dynamics for a variety of colloidal structures are needed in order to move the field forward. Hot electron relaxation in bulk metal films has been studied using photoelectron spectroscopy, 8,9 as well as transient reflectivity and transmission. 10-12 The electron-electron scattering process was determined to persist for approximately 500 fs for bulk gold.<sup>12</sup> However, accelerated electron-electron scattering rates are predicted for quantum-confined nanoparticles.  $^{13-15}$  This acceleration presents a challenge for resolving electron—electron scattering in nanoparticles by use of conventional transient spectroscopies. This complication is two-fold: (1) the accelerated lifetimes require broad bandwidth laser pulses, sacrificing spectral resolution, and (2) the inherent size inhomogeneity of colloidal nanoparticles limits typical ensemble measurements to resolving only inhomogeneous line widths  $(\Gamma_{ih}).^{16}$  Hence, a method that can simultaneously provide both high temporal resolution and yield the sample homogeneous line width  $(\Gamma_h)$  for colloidal ensembles is needed.

In this Letter, we describe the basis for using the time-dependent plasmon homogeneous line width  $(\Gamma_h(t))$  obtained from time-resolved two-dimensional electronic spectroscopy (2DES) measurements to study hot electron dynamics in metal nanostructures. The advantage of the 2DES approach is that whereas one-dimensional ensemble transient spectroscopy yields only the material inhomogeneous line width  $(\Gamma_{ih})$ , two-dimensional spectroscopy provides both  $(\Gamma_h)$  and  $(\Gamma_{ih})$ . Further, the pump–probe platform of ultrafast 2DES allows the time dependence of  $(\Gamma_h)$  to be obtained. We note that while single-particle measurements provide the

Received: August 10, 2020
Revised: September 14, 2020
Published: September 15, 2020





instantaneous  $(\Gamma_h(0))$  and conventional femtosecond transient spectroscopies give time-dependent  $(\Gamma_{ih}(t))$ , neither of these approaches produce the time-dependent  $(\Gamma_h(t))$  needed to track e—e scattering. The remainder of this Letter is organized as follows: (1) we first describe the theoretical framework of  $\Gamma_h$  probing by 2DES in the context of metallic electronic excitation and energy relaxation; (2) experimental details of the 2DES measurements are also provided; and (3) examples of electron—electron scattering processes in gold nanorods (AuNRs) are provided, followed by concluding remarks.

The instantaneous plasmon line width  $(\Gamma_h)$  is determined by the electronic dephasing processes typical for the metal, which for gold includes contributions from intrinsic "bulk" scattering  $(\gamma_b)$ , interband  $(\gamma_{ib})$ , radiative  $(\gamma_r)$ , and interface scattering  $(\gamma_{if})$ process, such that  $\Gamma_h = \gamma_b + \gamma_{ib} + \gamma_r + \gamma_{if}^{7,23}$  Because plasmon coherence times typically persist for 10 fs, or less, the instantaneous  $\Gamma_h$  is usually on the order of hundreds of millielectronvolts. <sup>23–26</sup> Moreover, because the plasmon coherence times are much shorter than the subsequent electronic relaxation processes of nonequilibrium electrons,  $\Gamma_h$  provides a static snapshot of electronic thermalization events occurring on the hundreds of femtoseconds to picoseconds time frame. Before excitation  $(t_2 < 0)$ , the conduction band electrons in the metal follow an energy-dependent Fermi-Dirac distribution,  $f(E) = \frac{1}{1 + e^{(E-E_{\rm F})/kT}}$ , where  $E_{\rm F}$  represents the Fermi energy, k is the Boltzmann constant, E is the thermal energy of the system, and T is the electron temperature, which should initially equal the lattice and laboratory temperatures. 27,28 This equilibrium energy distribution is depicted in the top panel of Figure 1. In the time frame following impulsive excitation but prior to the completion of electron–electron scattering ( $t_{e-e} \ge t_2 > 0$ ), the absorbed photon energy will modify the electron distribution, as shown in Figure 1b, by increasing the total energy of the electron gas. The newly created nonequilibrium carriers will be

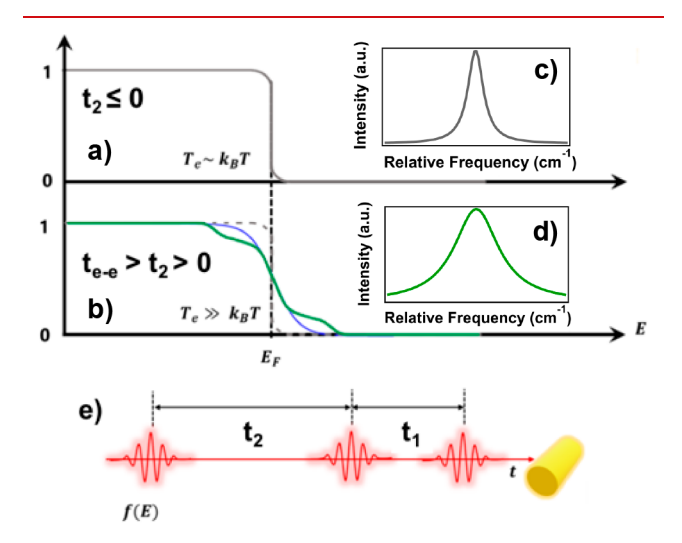


Figure 1. Overview of homogeneous line width analysis by 2DES. (a) Fermi–Dirac distribution of electrons in gold nanorods (AuNRs) before excitation. (b) Nonequilibrium distribution of excited electrons (green) and hot Fermi–Dirac distribution after energy redistribution among electrons through e–e scattering (blue). The gray line is electron distribution at room temperature, and the vertical black dash line indicates the Fermi energy level. Conceptual depictions of the corresponding plasmon homogeneous line widths at room temperature (c) and nonequilibrium electrons (d). (e) Pulse sequence for 2DES measurement.

distributed, depending on the excitation photon energy  $(h\nu)$ , as  $\pm h\nu$  with respect to the Fermi level. <sup>10–13</sup> Because the carrier density at the Fermi level is reduced by photoexcitation, the various dephasing mechanisms contributing to  $\Gamma_h$  will be accelerated. This acceleration results in transient broadening of  $\Gamma_{\rm h}$ , as depicted schematically in Figure 1c,d. These nonequilibrium carriers will relax via available sp conduction band states within hundreds of femtoseconds through electronelectron scattering. Next, the hot electron gas will transfer energy to the laboratory-temperature lattice through subpicosecond electron–phonon scattering. These relaxation steps result in time-dependent narrowing of  $\Gamma_{\rm h}$ . We note that impulsive laser excitation of the metal transiently alters the material dielectric properties, and hence also contributes to the line width on these time scales. Specifically, the rapid change in electron temperature modifies the intraband contribution to the imaginary component of the material dielectric for frequencies lower than the intraband resonance. We expect this excitation-induced dielectric change to be a significant source of line broadening, given that our measurements were conducted using frequencies lower than the intraband transition. Our interest here is to quantify the dynamics leading to the formation and decay of the nonequilibrium hot electron gas on the hundreds of femtoseconds time scale by analyzing the time-dependent plasmon homogeneous line width. This can be accomplished using 2DES, as long as the temporal duration of the excitation and detection laser pulses are shorter than or comparable to the plasmon coherence time.

The 2DES method is depicted in Figure 1e. A sequence of three temporally separated laser pulses are employed in these experiments. The first two laser pulses, separated by time delay  $t_1$ , are phase stabilized and used to generate the excitation axis of the 2DES maps; the excitation axis is produced by Fourier transformation of transient signals collected for a series of  $t_1$ time delays. Following excitation by the pulse pair, the dynamics are monitored by the transient extinction of a third, temporally delayed  $(t_2)$  probe pulse. The 2DES detection axis is obtained by dispersing the probe pulse on a spectrometer. A detailed description of the 2DES instrument can be found elsewhere.<sup>29</sup> Briefly, the 1040 nm fundamental pulses from a solid-state Yb amplifier (Spirit; Spectra Physics) were modulated to a 100 kHz repetition rate and sent to a noncollinear optical parametric amplifier (NOPA) to generate pulses in the visible wavelength range. The NOPA output (typically 720 nm center wavelength with a bandwidth of 45 nm) was collimated and sent to a pulse shaper-based 2DES spectrometer (PhaseTech). A 90/10 beam splitter divided the beam into two paths. The 10% reflected beam was first compressed using dispersion-compensating mirrors (DCM) then focused and directed to the sample. The 90% transmitted beam was dispersed using a grating then collimated by a parabolic mirror and guided to an acousto-optic modulator (AOM). The AOM was modulated to convert the input pulse into a two-pulse sequence with a controllable time-delay up to 5 ps  $(t_1)$ . A parabolic mirror then reflected the modulated pump pulse sequence, and the pulses were collected using a second grating and transformed back into the time domain. The overall geometry of a two-grating, two-parabolic mirror layout follows the 4 f geometry. A half-wave plate/polarizer pair was used to control the polarization of the pump pulse; in the experiment described here, the polarization of the pump beam was set to s-polarized, perpendicular to that of the probe beam. The pump pulses were delayed by a time delay  $(t_2)$ 

using a mechanical stage with step-size of 1 fs then focused and spatially overlapped with probe pulse at the sample.

The ensemble room-temperature linear extinction spectrum (solid black) of a colloidal AuNR sample (length-to-diameter aspect ratio =  $2.9 \pm 0.4$ ) is compared to several dark-field scattering (DFS) spectra measured at the single-particle level (Figure 2). The synthesis and characterization of the AuNRs

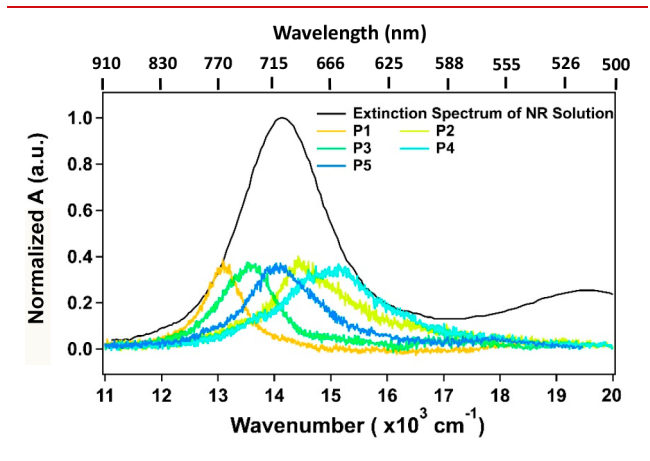


**Figure 2.** Comparison of AuNR ensemble and single-nanoparticle optical measurements. The extinction spectrum of colloidal AuNR ensemble solution (black) is plotted and overlaid with five representative dark-field scattering (DFS) spectra from single AuNR measurements (P1–P5). The DFS spectra were normalized to each other.

have been described elsewhere.<sup>30</sup> Two AuNR surface plasmon resonance (SPR) modes were evident in the ensemble spectrum: (1) a transverse (TSPR) mode at approximately 19 500 cm<sup>-1</sup> and (2) a longitudinal (LSPR) one at lower frequencies. Owing to the laser tuning range, the TSPR mode is not discussed further. The Figure 2 overlay illustrates the inhomogeneous broadening that dominates the ensemble LSPR peak width, resulting in  $\Gamma_{ih}$  of approximately 2400 cm<sup>-1</sup> with a mean extinction frequency of 14 200 cm<sup>-1</sup>. The single-AuNR DFS spectra reveal a distribution of LSPR frequencies that span the ensemble peak. The single-particle measurements provide the instantaneous homogeneous line width for each individual AuNR and span the range from 1000 to 1800 cm<sup>-1</sup>. These homogeneous line widths relate to the plasmon coherence time  $(\tau_p)$  as  $\tau_p = \frac{2\hbar}{\Gamma_h}$ , where  $\Gamma_h$  is determined from full width at half-maximum Lorentzian line fitting of the DFS spectra. <sup>22</sup> Using this conversion,  $\tau_{\rm p}$  values ranged from 6 to 11 fs, corresponding to  $\Gamma_h$  of 1800 and 1000 cm<sup>-1</sup>, respectively. These values were in excellent agreement with previous DFS and interferometry measurements on single AuNRs and were consistent with expectations based on known plasmon dephasing processes, described above. 23-26

Next, the response of the time-dependent change in the homogeneous line width to excitation pulse energy (i.e., pump power) is described. These experiments were conducted using a broad bandwidth ( $\Delta\omega=860~{\rm cm}^{-1}$ ) femtosecond laser pulse with a carrier wave frequency of 13 900 cm<sup>-1</sup> (720 nm). Following compression, an approximate 12 fs pulse duration was achieved, which matched well with the plasmon coherence times obtained from the Figure 2 DFS data. Hence, the laser pulse was selected to coherently excite and probe the plasmon resonance of a subpopulation of the ensemble. A representative 2DES map obtained at a pump—probe time delay of 100 fs and

5.7 nJ pulse energy is shown in Figure 3a. The 2DES map was dominated by a transient bleach signal extended along the

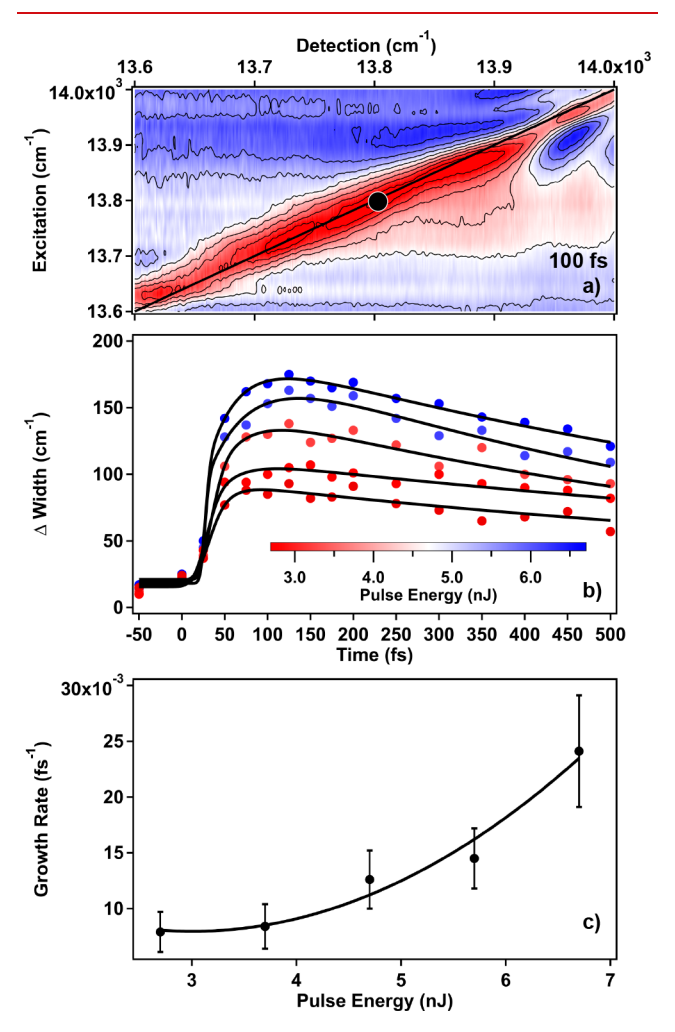


**Figure 3.** (a) The 2DES spectrum of AuNRs recorded at a pump—probe time delay of 100 fs using 5.7 nJ pulses with carrier wave frequencies of 13 900 cm<sup>-1</sup> (720 nm). (b) Overlay of the change of the AuNR longitudinal surface plasmon (LSPR) homogeneous width plotted versus pump—probe waiting time for excitation pulse energies spanning 2.7–6.7 nJ/pulse. Line widths were analyzed at excitation/detection frequencies of 13 800 cm<sup>-1</sup>. (c) The rate of LSPR homogeneous line width broadening, obtained from fitting panel b data, plotted versus excitation pulse energy. A quadratic excitation pulse energy dependence was obtained.

diagonal; increasing bleach magnitude is depicted in red. In order to examine the sensitivity of  $\Gamma_{\rm h}(t)$  to laser excitation fluence, the homogeneous line width (i.e., the width perpendicular to the diagonal) was quantified by Lorentzian fitting for a series of laser pulse energies at multiple pump—probe time delays spanning 0–500 fs. We note that a low-amplitude off-diagonal signal was also detected. The contribution of this component to the transient bleach signal was accounted for by the inclusion of a Gaussian function (Figure S1). The Gaussian component accounted for approximately five percent of the total transient signal (Figure S2). The line width change observed at 13 800 cm<sup>-1</sup> using five different excitation pulse energies, spanning 2.7–6.7 nJ, is plotted versus the pump—probe time delay in Figure 3b. These excitation pulse energies correspond to photoinduced changes

Table 1. Pump Power-Dependent Peak Broadening Growth Fit Results

pulse energy (nJ)	2.7	3.7	4.7	5.7	6.7
growth time (fs)	$130 \pm 25$	$120 \pm 15$	$80 \pm 10$	$70 \pm 10$	$45 \pm 10$
rate constant (fs <sup>-1</sup> )	0.008 + 0.001	0.008 + 0.001	0.013 + 0.001	0.014 + 0.002	0.022 + 0.003

of the electron temperature that spanned ~600 K (2.7 nJ) to 1600 K (6.7 nJ).  $^{31,32}$  The time dependence of the change in line width is described by an initial increase (line broadening) and subsequent reduction (line narrowing). Following thermalization, the LSPR line width returns to the equilibrium  $\Gamma_{\rm h}$  value (Figure S1). The maximum line width broadening measured in these experiments spanned the range from 80 cm $^{-1}$  (2.7 nJ/pulse) to 180 cm $^{-1}$  (6.7 nJ/pulse), depending on the excitation pulse energy. Considering the highest pulse energies used, the 180 cm $^{-1}$  increase in LSPR width corresponds to an approximately 2 fs reduction in the plasmon coherence time (i.e.,  $\tau_{\rm p}=9$  fs). Although a seemingly small change, the broadened line width corresponded to an approximately 20% increase in the plasmon dephasing rate upon excitation of the electron gas.

Qualitatively, the line broadening step was complete within approximately 150 fs, while the subsequent line narrowing process persisted for hundreds of femtoseconds. The line narrowing time constant increased linearly with excitation pulse energy (Figure S3), spanning the range from  $620 \pm 50$  fs (2.7 nJ) to  $970 \pm 60 \text{ fs } (6.7 \text{ nJ})$ . These time scales matched expectations for electron-electron (150 fs) and electronphonon scattering processes (hundreds of femtoseconds). 14,15 These time-dependent changes to the line width were fit quantitatively using a consecutive kinetics model that included a first-order growth and a subsequent first-order decay. The fitting results for the line broadening step are given in Table 1 and plotted versus excitation energy in Figure 3c. For the lowest excitation pulse energy used (2.7 nJ), the time constant of the electron-electron scattering step was 130  $\pm$  20 fs. Increases in pulse energy accelerated the electron-electron scattering rate, yielding a time constant of  $45 \pm 10$  fs for 6.7 nJ/pulse excitation. A plot of the resultant electron-electron scattering rates versus excitation pulse energy is described by a quadratic function (Figure 3c). We note that this quadratic excitation power dependence is consistent with expectations for electron-electron scattering rates based on Fermi-liquid theory, 27,33,34 which predicts quadratic dependences of electron-electron scattering on both excitation energy and electron temperature. Specifically, the temperature dependence of the electron-electron,  $k_{ee}$ , scattering rate is approximated as  $k_{\rm ee} \propto (T_{\rm e})^2$  where  $T_{\rm e}$  is the electron temperature.<sup>34</sup> As described above, the range of excitation pulse energies used in these experiments correspond to increased T<sub>e</sub> values spanning 600-1600 K. We extend this study by considering the excitation frequency dependence of the electron-electron

Next, the excitation frequency dependence of the homogeneous line width broadening is described. The line width was analyzed at a series of excitation/detection frequencies (13.70, 13.75, 13.80, 13.85, 13.90  $\times$   $10^3~cm^{-1})$  distributed along the 2DES diagonal (Figure 4a). A pulse energy of 5.7 nJ was used for all excitation frequencies. The resultant changes in the homogeneous line width are plotted in Figure 4b. Similar to the excitation pulse energy, the greatest excitation frequency resulted in the largest increase in the homogeneous line width  $(\Delta\Gamma_h\approx 400~cm^{-1}$  at  $14\,200~cm^{-1}$  excitation frequency). The

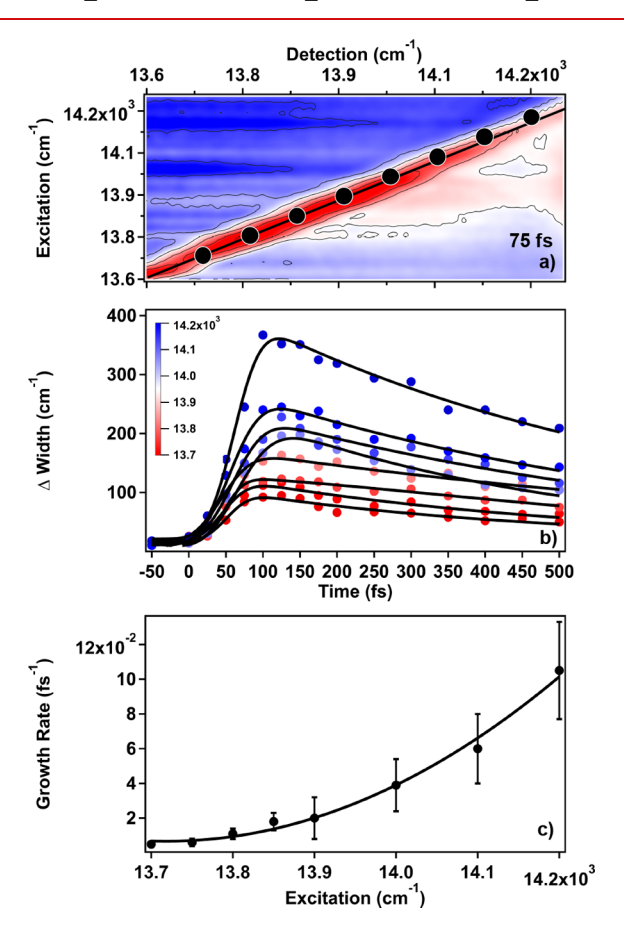


**Figure 4.** (a) The 2DES spectrum of AuNRs recorded at a pump—probe time delay of 75 fs using 5.7 nJ pulses with carrier wave frequency of 13 900 cm<sup>-1</sup> (720 nm), spanning the range 13 600—14 200 cm<sup>-1</sup>. (b) Overlay of the change of the AuNR longitudinal surface plasmon (LSPR) homogeneous width plotted versus pump—probe waiting time for excitation pulse frequencies spanning 13 700—14 200 cm<sup>-1</sup>. Line widths were analyzed at excitation pulse energies of 5.7 nJ. (c) The rate of LSPR homogeneous line width broadening, obtained from fitting panel b data, plotted versus excitation pulse frequency. A quadratic excitation pulse energy dependence was obtained.

lowest excitation frequency (13 700 cm<sup>-1</sup>) produced a 100 cm<sup>-1</sup> line width increase. The changes in line widths corresponded to an acceleration of the plasmon dephasing time that increased monotonically from 10% to 50% as the excitation frequency was increased from 13 700 to 14 200 cm<sup>-1</sup>. The observed excitation frequency dependence of the coherence times was expected because the plasmon decoherence rates were accelerated by the increased density of unoccupied Fermi-level states following impulsive excitation. The line width broadening and narrowing rates were also quantified using the consecutive kinetics model described for the pulse energy dependence. The fit results are shown using solid lines in Figure 4b. The resultant rates for homogeneous line width broadening are plotted versus the excitation frequency in Figure 4c (Table 2). Similar to the pulse-energy

Table 2. Excitation Energy-Dependent Peak Broadening Growth Fit Results

energy $(10^3 \text{ cm}^{-1})$	13.7	13.75	13.80	13.85	13.90	14.00	14.10	14.20
growth time (fs)	$200\pm40$	$140\pm20$	$90 \pm 10$	$55 \pm 10$	$50 \pm 10$	$25 \pm 10$	$15 \pm 10$	$10 \pm 5$
rate constant	$0.005 \pm 0.001$	$0.007 \pm 0.002$	$0.011 \pm 0.003$	$0.018 \pm 0.005$	$0.02 \pm 0.01$	$0.04 \pm 0.015$	$0.067 \pm 0.02$	$0.100 \pm 0.02$

dependence, the line broadening rates increased quadratically with excitation frequency.

The quadratic dependences on both the excitation pulse energy and frequency can be understood by considering Fermiliquid theory. In this model, the energy redistribution time for one electron with energy E should be proportional to energy

difference 
$$\Delta E = E_{hv} - E_{F}$$
, as  $k_{e-e} = \tau_0^{-1} \left(\frac{\Delta E}{E_F}\right)^2$ , where  $E_F$ 

represents the Fermi energy level,  $E_{hv}$  is the excitation energy (frequency), and  $\tau_0^{-1}$  is the intrinsic electron–electron scattering rate of the material. 15,31 Although this equation is derived for zero temperature, the quadratic relation between the electron–electron scattering time and  $\Delta E$  still holds at kTand higher temperatures.<sup>27</sup> This is true because the photoinduced electron-electron interactions do not alter the freeelectron nature of the metal as a result of the exclusion principle. Thus, nonequilibrium electron-electron scattering dynamics in AuNRs can be accurately described by Fermiliquid theory. As our experimental results show, increased excitation energy and frequency both resulted in the promotion of electrons to higher energy states above the Fermi-level; the higher excitation energy corresponded to larger excess electron energies. Consistent with Fermi-liquid theory, this excess energy resulted in accelerated electronelectron relaxation rates.

The Figure 3 data were used to determine the intrinsic electron-electron scattering time constants,  $\tau_0$ , of the nanorods, which yielded  $\tau_0 = 230 \pm 40$  fs. We note that this time is slightly faster than but comparable to those previously reported for smaller metal nanoparticles. Silver nanospheres (~2 nm radius) exhibit electron-electron scattering time constants of 150 fs, that increase monotonically with radius, saturating at 350 fs for 13 nm radius particles. 15 A similar trend is observed for gold nanoparticles, but with maximal time constants of ~500 fs. Our measurements were extended to include 2.5 nm radius and 5 nm radius gold nanospheres (Figure S4), which yielded  $\tau_0$  = 375  $\pm$  50 fs and 405  $\pm$  50 fs, respectively. These values are well within the expected range for metal nanoparticles of this size and confirm that the 2DES method can be reliably used to resolve electron-electron scattering in plasmonic ensembles. Further studies will be needed to understand the mechanism of accelerated electronelectron scattering in nanorods.

In this Letter, we described the use of femtosecond time-resolved 2DES to analyze the electronic relaxation dynamics of photoexcited AuNRs. This was accomplished by monitoring the time-dependent plasmon homogeneous line width ( $\Gamma_h$ ) obtained from 2DES measurements. We demonstrated that plasmon-resonant excitation resulted in a broadening of  $\Gamma_h$  that corresponded to a 20–50% acceleration of the plasmon dephasing time, depending on the excitation conditions. This acceleration was caused by changes in the Fermi-level carrier density. Because these changes occur on the sub-10 fs time frame, the time dependence of  $\Gamma_h$  could be used to track subsequent electronic relaxation processes occurring on longer time scales. Specifically, this approach provided access to the

difficult to resolve electron-electron scattering dynamics of a colloidal AuNR ensemble. The time, excitation pulse energy, and frequency dependence of the homogeneous line width were consistent with expectations based on Fermi-liquid theory; the line broadening time constants were typically on the order of 100 fs and increased quadratically with increases to both the excitation pulse energy and frequency. The ability to resolve the time-dependent broadening of  $\Gamma_h$  from 2DES measurements allows for experimental investigation of the mechanisms of hot carrier generation in plasmonic metals. We anticipate that this experimental approach will provide valuable information regarding hot electron dynamics and interfacial carrier transfer for metallic nanoparticle and metal-containing heterostructures. Outcomes from this research could provide important insights for the design of metal-based transducers, including photocatalysts.

## ASSOCIATED CONTENT

# **Supporting Information**

The Supporting Information is available free of charge at https://pubs.acs.org/doi/10.1021/acs.nanolett.0c03272.

The 2DES maps representing a series of antidiagonal line width profiles, fitting results of the antidiagonal line width profiles, Gaussian and Lorentzian fit coefficients, summary of time constants for the homogeneous line width  $(\Gamma_{\rm h})$  changes versus excitation pulse energy for gold nanorods, intrinsic  $\tau_0$  values for gold nanospheres with 2.5 and 5 nm radii (PDF)

# AUTHOR INFORMATION

## **Corresponding Author**

Kenneth L. Knappenberger, Jr. – Department of Chemistry, The Pennsylvania State University, University Park, Pennsylvania 16802, United States; ⊙ orcid.org/0000-0003-4123-3663; Email: klk260@psu.edu

### **Authors**

William R. Jeffries – Department of Chemistry, The Pennsylvania State University, University Park, Pennsylvania 16802, United States

**Kyoungweon Park** — Air Force Research Laboratory, Wright-Patterson Air Force Base, Ohio 45433, United States; orcid.org/0000-0001-8069-3000

Richard A. Vaia — Air Force Research Laboratory, Wright-Patterson Air Force Base, Ohio 45433, United States;
ocid.org/0000-0003-4589-3423

Complete contact information is available at: https://pubs.acs.org/10.1021/acs.nanolett.0c03272

### Notes

The authors declare no competing financial interest.

## ACKNOWLEDGMENTS

K.L.K. and W.R.J. received funding from the Air Force of Scientific Research (FA9550-18-1-0347) and from the Na-

tional Science Foundation (CHE-1807999). We acknowledge Hongjun Zheng for assistance with measurements.

## REFERENCES

- (1) Mukherjee, S.; Libisch, F.; Large, N.; Neumann, O.; Brown, L.; Cheng, J.; Lassiter, J. B.; Carter, E.; Nordlander, P.; Halas, N. Hot Electrons Do the Impossible: Plasmon-Induced Dissociation of H<sub>2</sub> on Au. *Nano Lett.* **2013**, *13*, 240–247.
- (2) Furube, L. A.; Hashimoto, S. NPG Asia Mater. 2017, 9, No. e454.
- (3) Furube, A.; Du, L.; Hara, K.; Katoh, R.; Tachiya, M. Ultrafast Plasmon-Induced Electron Transfer from Gold Nanodots into  ${\rm TiO_2}$  Nanoparticles. *J. Am. Chem. Soc.* **2007**, *129*, 14852-13853.
- (4) Christopher, P.; Xin, H.; Marimuthu, A.; Linic, S. Singular Characteristics and Unique Chemical Bond Activation Mechanisms of Photocatalytic Reactions on Plasmonic Nanostructures. *Nat. Mater.* **2012**, *11*, 1044–1050.
- (5) Zhang, X.; Li, X.; Reish, M. E.; Zhang, D.; Su, N. Q.; Gutierrez, Y.; Moreno, F.; Yang, W.; Everitt, H. O.; Liu, J. Plasmon-Enhanced Catalysis; Distinguishing Thermal and Nonthermal Effects. *Nano Lett.* **2018**, *18*, 1714–1723.
- (6) Cushing, S. K.; Li, J.; Meng, F.; Senty, T. R.; Suri, S.; Zhi, M.; Li, M.; Bristow, A. D.; Wu, N. Photocatalytic Activity Enhanced by Plasmonic Resonant Energy Transfer from Metal to Semiconductor. J. Am. Chem. Soc. 2012, 134, 15033–15041.
- (7) Hartland, G. V. Optical Studies and Dynamics of Noble Metal Nanostructures. *Chem. Rev.* **2011**, *111*, 3858–3887.
- (8) Fann, W. S.; Storz, R.; Tom, H. W. K.; Bokor, J. Electron Thermalization in Gold. *Phys. Rev. B: Condens. Matter Mater. Phys.* 1992, 46, 13592–13595.
- (9) Fann, W. S.; Storz, R.; Tom, H. W. K.; Bokor, J. Direct Measurement of Nonequilibrium Electron-Energy Distributions in Subpicosecond Laser-heated Gold Films. *Phys. Rev. Lett.* **1992**, *68*, 2834–2837.
- (10) Sun, C. K.; Vallée, F.; Acioli, L.; Ippen, E. P.; Fujimoto, J. G. Femtosecond Investigation of Electron Thermalization in Gold. *Phys. Rev. B: Condens. Matter Mater. Phys.* **1993**, 48, 12365–12368.
- (11) Sun, C. K.; Vallée, F.; Acioli, L. H.; Ippen, E. P.; Fujimoto, J. G. Femtosecond- Tunable Measurement of Electron Thermalization in Gold. *Phys. Rev. B: Condens. Matter Mater. Phys.* **1994**, *50*, 15337–15348.
- (12) Del Fatti, N.; Voisin, C.; Achermann, M.; Tzortzakis, S.; Christofilos, D.; Vallée, F. Nonequilibrium Electron Dynamics in Noble Metals. *Phys. Rev. B: Condens. Matter Mater. Phys.* **2000**, *61*, 16956–16966.
- (13) Voisin, C.; Del Fatti, N.; Christofilos, D.; Vallée, F. Ultrafast Electron Dynamics and Optical Nonlinearities in Metal Nanoparticles. *J. Phys. Chem. B* **2001**, *105*, 2264–2280.
- (14) Voisin, C.; Christofilos, D.; Del Fatti, N.; Vallée, F.; Prével, B.; Cottancin, E.; Lermé, J.; Pellarin, M.; Broyer, M. Size-Dependent Electron-Electron Interactions in Metal Nanoparticles. *Phys. Rev. Lett.* **2000**, *85*, 2200.
- (15) Arbouet, A.; Voisin, C.; Christofilos, D.; Langot, P.; Fatti, N. D.; Vallée, F.; Lermé, J.; Celep, G.; Cottancin, E.; Gaudry, M.; Pellarin, M.; Broyer, M.; Maillard, M.; Pileni, M. P.; Treguer, M. Electron-Phonon Scattering in Metal Clusters. *Phys. Rev. Lett.* **2003**, 90. 177401.
- (16) Seferyan, H. Y.; Zadoyan, R.; Wark, A. W.; Corn, R. M.; Apkarian, V. A. Diagnostics of Spectrally Resolved Transient Absorption: Surface Plasmon Resonance of Metal Nanoparticles. *J. Phys. Chem. C* **2007**, *111*, 18525–18532.
- (17) Bristow, A. D.; Zhang, T.; Siemens, M. E.; Cundiff, S. T.; Mirin, R. P. Separating Homogenous and Inhomogeneous Line Widths of Heavy-and Light-Hole Excitons in Weakly Disordered Semiconductor Quantum Wells. *J. Phys. Chem. B* **2011**, *115*, 5365–5371.
- (18) Ginsberg, N. S.; Cheng, Y. C.; Fleming, G. R. Two-Dimensional Electronic Spectroscopy of Molecular Aggregates. *Acc. Chem. Res.* **2009**, *42*, 1352–1363.

- (19) Gellen, T. A.; Lem, J.; Turner, D. B. Probing Homogeneous Line Broadening in CdSe Nanocrystals Using Multidimensional Electronic Spectroscopy. *Nano Lett.* **2017**, *17*, 2809–2815.
- (20) Seiler, H.; Palato, S.; Sonnichsen, C.; Baker, H.; Kambhampati, P. Seeing Multiexcitons through Sample Inhomogeneity: Band-Edge Biexciton Structure in CdSe Nanocrystals Revealed by Two-Dimensional Electronic Spectroscopy. *Nano Lett.* **2018**, *18*, 2999–3006
- (21) Lietard, A.; Hsieh, C. S.; Rhee, H.k.; Cho, M. Electron Heating and Thermal Relaxation of Gold Nanorods Revealed by Two-dimensional Electronic Spectroscopy. *Nat. Commun.* **2018**, *9*, 891.
- (22) Seiler, H.; Palato, S.; Sonnichsen, C.; Baker, H.; Socie, E.; Strandell, D.; Kambhampati, P. Two-dimensional Electronic Spectroscopy Reveals Liquid-like Lineshape Dynamics in CsPbI<sub>3</sub> Perovskite Nanocrystals. *Nat. Commun.* **2019**, *10*, 4962.
- (23) Link, S.; El-Sayed, M. A. Size and Temperature Dependence of the Plasmon Absorption of Colloidal Gold Nanoparticles. *J. Phys. Chem. B* **1999**, *103*, 4212–4217.
- (24) Sonnichsen, C.; Franzl, T.; Wilk, T.; von Plessen, G.; Feldmann, J.; Wilson, O.; Mulvaney, P. Drastic Reduction of Plasmon Damping in Gold Nanorods. *Phys. Rev. Lett.* **2002**, *88*, 4.
- (25) Fang, Y.; Chang, W. S.; Willingham, B.; Swanglap, P.; Dominguez-Medina, S.; Link, S. Plasmon Emission Quantum Yield of Single Gold Nanorods as a Function of Aspect Ratio. *ACS Nano* **2012**, *6*, 7177–7184.
- (26) Jarrett, J. W.; Zhao, T.; Johnson, J. S.; Knappenberger, K. L. Investigating Plasmonic Structure-Dependent Light Amplification and Electronic Dynamics Using Advances in Nonlinear Optical Microscopy. *J. Phys. Chem. C* **2015**, *119*, 15779–15800.
- (27) Ashcroft, N. W.; Merriman, N. D. Solid State Physics; Holt, Rinehart and Winston: New York, 1976.
- (28) Kaganov, M. I.; Lifshitz, I. M.; Tanatarov, L. V. Relaxation between electrons and the crystalline lattice. *Sov. Phys. JETP* **1957**, 4 (2).
- (29) Steves, M. A.; Zheng, H.; Knappenberger, K. L., Jr. Correlated Spatially Resolved Two-dimensional Electronic and Linear Absorption Spectroscopy. *Opt. Lett.* **2019**, *44*, 2117–2120.
- (30) Park, K.; Hsiao, M.-s.; Yi, Y.-J.; Izor, S.; Koerner, H.; Jawaid, A.; Vaia, R. A. ACS Appl. Mater. Interfaces 2017, 9, 26363–26371.
- (31) Ferrera, M.; Della Valle, G.; Sygletou, M.; Magnozzi, M.; Catone, D.; O'Keeffe, P.; Paladini, A.; Toschi, F.; Mattera, L.; Canepa, M.; Bisio, F. Thermometric Calibration of the Ultrafast Relaxation Dynamics in Plamonic Au Nanoparticles. *ACS Photonics* **2020**, *7*, 959–966.
- (32) Rouxel, R.; Diego, M.; Medeghini, F.; Maioli, P.; Rossella, F.; Vallée, F.; Banfi, F.; Crut, A.; Del Fatti, N. Ultrafast Thermo-Optical Dynamics of a Single Metal Nano-Object. *J. Phys. Chem. C* **2020**, *124*, 15625–15633.
- (33) Pines, D.; Nozieres, P. The Theory of Quantum Liquids: Normal Fermi liquids; CRC Press: Boca Rata, FL, 1989.
- (34) Tsuei, C. C.; Gupta, A.; Koren, G. Quadratic Temperature Dependence of the In-Plane Resistivity in Superconducting Nd1.85CuO4 Evidence for Fermi-Liquid Normal State. *Phys. C* **1989**, *161*, 415–422.